AIAA JOURNAL
Vol. 38, No. 4, April 2000

Trailing-Edge Noise Prediction Using Large-Eddy Simulation and Acoustic Analogy

Eric Manoha,* Bruno Troff,* and Pierre Sagaut*
ONERA, 92320 Châtillon, France

The filtered Navier–Stokes equations are used to perform the large-eddy simulation of the unsteady incompressible flow around the blunt trailing edge of a thick flat plate. The computed flow exhibits a three-dimensional vortex shedding mechanism. The frequency domain of this mechanism is in agreement with experiments and theory. In that frequency domain normalized wall-pressure levels are favorably compared to spectra measured at the blunted trailing edge of an airfoil. The far-field radiated noise is first computed via Curle's formulation, the solution of Lighthill's equation for flows embedding solid bodies. Then the theory developed by Ffowcs Williams and Hall is considered. This formulation expresses the noise generated by turbulence passing over the edge of an infinite half-plane. The suitability of this theory to the case for a thick plate is discussed. The normalized spectra of the radiated noise predicted by both methods are compared, in the frequency domain of the vortex-shedding mechanism, to airfoil noise measurements in an anechoic facility.

Nomenclature

C_f	= wall friction coefficient
c	= speed of sound
$\boldsymbol{f}$	= force per unit area exerted on the fluid by solid surfaces (components f_i)
$G(\boldsymbol{x} \mid \boldsymbol{y}, \omega)$	= acoustic Green's function: radiated noise at the observation point $\boldsymbol{x}$ caused by a harmonic monopole at the point source $\boldsymbol{y}$
H	= trailing-edge thickness
k	= acoustic wave number ω/c
$\boldsymbol{m}$	= subgrid-scale stress tensor
p	= instantaneous pressure
$\bar{p}$	= instantaneous filtered normalized pressure, $p/\rho U_\infty^2$
q	= fluctuating kinetic energy
R	= distance between the observation point $\boldsymbol{x}$ and the point source $\boldsymbol{y}$
Re_H	= Reynolds number, $U_\infty H/\nu$
t_w	= wake thickness, $H + 2\delta^*$
$\boldsymbol{U}$	= mean fluid velocity
U_∞	= external velocity
$\boldsymbol{u}$	= instantaneous fluid velocity
$\bar{\boldsymbol{u}}$	= instantaneous filtered normalized velocity
u_τ	= friction velocity, $U_\infty \sqrt{(C_f/2)}$
u^+, z^+	= wall units, u/u_τ and zu_τ/ν, respectively
$\bar{\Delta}$	= characteristic length scale of the grid filter $(\Delta x \Delta y \Delta z)^{1/3}$
δ	= boundary-layer thickness
$\delta(\boldsymbol{x})$	= spatial Dirac function
δ^*	= boundary-layer displacement thickness
θ	= boundary-layer momentum thickness
μ	= dynamic fluid viscosity
ν	= kinematic fluid viscosity, μ/ρ
ν_{SM}	= subgrid-scale viscosity
Π	= modified pressure, $\bar{p} + \frac{1}{3} m_{kk} I$
ρ	= density
ω	= frequency
$\langle\rangle$	= time average

I. Introduction

THIS numerical study is related to the general topic of airframe noise reduction. The engine noise and the aerodynamic noise of large airliners in landing configuration are now of the same order of magnitude. The aerodynamic noise is mostly generated by aeroacoustic sources such as landing gear and high-lift devices. In this context trailing-edge noise appears as one of the fundamental aeroacoustic mechanism for which there exists a strong demand for reliable prediction tools.

Trailing-edge noise can have different origins. On a rigid airfoil with a sharp trailing edge, acoustic diffraction of the turbulence passing the trailing edge generates broadband noise. In the case of a blunt trailing edge, the vortex-shedding mechanism adds a narrowband frequency noise. Moreover, both mechanisms may contribute to the vibrations of a flexible airfoil, with the consequences of radiated noise and structural fatigue.

Modeling of these mechanisms has received considerable attention in the past: a complete review of the existing models for trailing-edge noise was given by Howe,[1] and the noise radiated by airfoils with both sharp and bluff trailing edges was extensively studied by Brooks and Hodgson[2] and Garcia.[3] However, practical use of these models has long been limited by the considerable difficulty of providing them with reliable and comprehensive data describing turbulent flows, such as fluid velocity and wall-pressure fluctuations. The continuing progress of computational fluid dynamics techniques and computer performance makes such information readily accessible, allowing the rapid development of computational aeroacoustics (CAA).

Complete simultaneous numerical computation of both near-field turbulent flow and far-field radiated noise requires computer capabilities so far unavailable. Such computations are still limited to very simple two-dimensional geometries[4,5] but are very helpful for understanding physical mechanisms and validating more practical hybrid methods in which the near-field flow and the far-field noise are computed separately. Tam[6] and Lele[7] have recently given reviews of such methods including Kirchhoff surface[8] and acoustic analogy.[9–12]

In the present work a hybrid method combining large-eddy simulation (LES) and Lighthill's acoustic analogy[13,14] is used to predict the noise radiated by the blunt trailing edge of a flat plate.[15,16]

The paper first describes the LES of the incompressible flow computed using the PEGASE code developed at ONERA. Then the resulting aerodynamic data are analyzed and compared to the theoretical features of such flows and to experimental data collected by ONERA on the trailing edge of an airfoil in an anechoic wind tunnel.[3]

Curle's formulation[17] is then numerically applied to the LES data. This formulation is an extension of the general free-field solution of Lighthill's equation to flows around solid bodies. The radiated sound is obtained by a quadrupolar volume integration and a dipolar surface integration. Then, the theory developed by Ffowcs Williams and Hall[18] is considered. This formulation provides the noise generated

Presented as Paper 98-1066 at the AIAA 36th Aerospace Sciences Meeting, Reno, NV, 12–15 January 1998; received 14 January 1998; revision received 23 September 1998; accepted for publication 16 August 1999.

*Research Engineer, Department of Computational Fluid Dynamics and Aeroacoustics, BP 72.

by turbulence passing over the edge of an infinite half-plane. The suitability of this formulation for the case of a thick plate is discussed.

The normalized spectra of the radiated noise predicted by both methods are compared, in the frequency domain of vortex-shedding mechanism to airfoil noise measurements performed by NASA in a quiet flow facility.[2]

II. LES

LES is performed with the PEGASE code developed at ONERA to compute transitional and separated flows.[19,20] Results already obtained with this code have shown that LES may be interesting for predicting the unsteady features of such flows.

A. Governing Equations

The filtered Navier–Stokes equations of an incompressible fluid are used. Considering the skew-symmetric form of the convection terms, the equations for the grid filter quantities $\bar{u}$ and Π can be written as

$$\frac{\partial \bar{u}}{\partial t} + \frac{1}{2}[\nabla \cdot (\bar{u} \otimes \bar{u}) + \bar{u} \cdot \nabla \bar{u}] = -\nabla \Pi + \frac{1}{Re}\nabla^2 \bar{u} - \nabla \cdot \boldsymbol{m} \quad (1)$$

$$\nabla \cdot \bar{u} = 0 \quad (2)$$

where $\boldsymbol{m} = \overline{u \otimes u} - \bar{u} \otimes \bar{u}$ is the subgrid-scale tensor. The modified pressure Poisson equation is obtained by taking the divergence of Eq. (1):

$$-\nabla^2 \Pi = \frac{\partial (\nabla \cdot \bar{u})}{\partial t} + \nabla \cdot \nabla \cdot (\bar{u} \otimes \bar{u}) + \nabla \cdot \nabla \cdot \boldsymbol{m} \quad (3)$$

B. Subgrid-Scale Model

The subgrid-scale (SGS) tensor model is achieved in the usual way by using a gradient diffusion hypothesis:

$$\boldsymbol{m} = -\nu_{\mathrm{SM}}(\nabla \bar{u} + \nabla^T \bar{u}) \quad (4)$$

The subgrid-scale viscosity ν_{SM} of this model is computed using the mixed scale model (MSM), developed at ONERA in collaboration with the Laboratoire d'Informatique pour la Mécanique et les Sciences de l'Ingénieur (LIMSI)[21]:

$$\nu_{\mathrm{SM}} = C_M(|\nabla \times \bar{u}|)^{\frac{1}{2}} q^{\frac{1}{4}} \bar{\Delta}^{\frac{3}{2}} \quad (5)$$

where the kinetic energy q at the cutoff frequency is approximated by the kinetic energy of a test field $(\bar{u})' = \bar{u} - \hat{\bar{u}}$, corresponding to the highest resolved frequencies. In practice, $\hat{}$ denotes a test filter with a characteristic cutoff length scale equal to $2\bar{\Delta}$. That contribution of the highest resolved frequencies to the subgrid viscosity ensures that the model will return a zero SGS viscosity when the flow is fully resolved and will vanish automatically in the viscous sublayer of boundary layers. In the present work $C_M = 0.1$.

C. Numerical Procedure

The governing equations are solved on a nonstaggered grid with a second-order accurate hybrid finite difference/finite element method. Time integration is performed with a second-order accurate semi-implicit Adams–Bashforth/Crank–Nicolson scheme. Details of the basic method and validation benchmarks are given in Ref. 22. The terms arising from the SGS model were discretized in conservative form with centered coupling second-order accurate 27-point stencil schemes. The modified pressure is calculated from Eq. (3) by a Jacobi-preconditioned Bi-CGSTAB iterative method.[23]

The computation domain shown in Fig. 1 is a rectangular domain embedding the trailing edge of an infinite flat plate of thickness H. To minimize the influence of boundary conditions, a large computational domain is used. The part of the flat plate included in the computational domain is $10H$ long in the streamwise direction. The downstream boundary is located $20H$ away from the trailing edge, and the upper and lower boundaries are $20H$ away from the plate. These values are greater than those generally used for the LES of wakes downstream of bluff bodies.[24] The size of the domain in the spanwise direction is set to $5H$. The resulting size of the computational domain is $30H \times 5H \times 40H$.

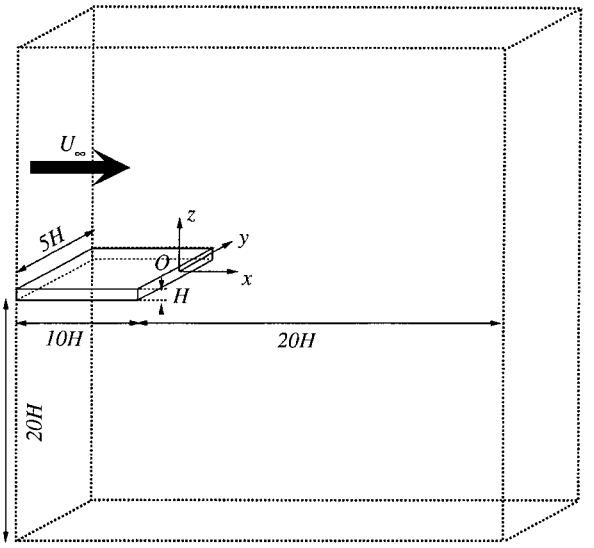

Fig. 1 Computation domain.

The simulation described here is performed on a nonuniform Cartesian grid. The horizontal plane $z = 0$ is a plane of symmetry, so that the following grid description only concerns the half-domain $z > 0$. In the spanwise direction y the grid cells have a constant size $\Delta y/H = 0.1$. In any (x, z) plane the four smallest cells, which dimensions are $\Delta x/H = \Delta z/H = 0.02$, are adjacent to the plate's corner $(x/H = 0, z/H = 0.5)$. With this arrangement the grid points nearest to the walls are located at a distance $\Delta x^+ = \Delta z^+ \approx 1$ (in wall units) from the plate, which makes it realistic to use a no-slip boundary condition, and allows the SGS model to vanish automatically at the wall, without an extra wall-damping function. From the plate's corner the grid is streched in the streamwise (upstream and downstream) direction x with a grid-stretching coefficient equal to 1.05 and in the transverse (up and down) direction z with a grid-stretching coefficient equal to 1.06. In both directions the ratio between the largest and the smallest cell sizes is equal to 57. The whole grid contains 161 points in x, 51 points in y, and 201 points in z, representing a total of 1.65×10^6 points.

The concept of grid convergence of the results, if well defined for direct numerical simulation (DNS) and Reynolds-averaged Navier–Stokes (RANS), is more problematic for LES because the filtering length scale is directly linked to the computational grid through Deardorff's formulas $\bar{\Delta} = (\Delta x \Delta y \Delta z)^{1/3}$. The natural grid-converged limit is then the DNS result.

The Reynolds number Re_H, based on the maximal inflow velocity and the plate thickness, is set equal to 1000.

A steady velocity field is imposed on the inflow boundary $(x/H = -10)$. The prescribed velocity field is obtained by superimposing 1) a boundary-layer profile for the streamwise velocity and 2) a three-dimensional perturbation, which is used to promote the onset of three-dimensional modes in the wake.

1) The streamwise velocity profile results from a DNS of the turbulent boundary layer (TBL) on a flat plate computed by Spalart.[25] The Reynolds numbers based on the TBL displacement thickness δ^* and momentum thickness θ are $Re_{\delta^*} = 2000$ and $Re_\theta = 1410$. The boundary-layer thickness is $\delta \approx 7.2\delta^*$, and the friction coefficient is $C_f = 0.0413$. This profile is presented in wall units $U_x^+ = f(z^+)$ in Fig. 2. On the logarithmic plot the profile is compared to the theoretical law-of-the-wall $U_x^+ = z^+$ in the range $0 < z^+ < 10$ and a logarithmic law in the range $10 < z^+ < 300$.

2) To generate realistic spanwise modes in the wake, three-dimensional vortical perturbations are imposed on the inflow boundary. By using hydrogen-bubble injection Smith and Schwartz[26] observed contrarotating vortices in TBLs with Reynolds numbers in the range $1000 < Re_\theta < 2200$. In their simulations Wakarami and Pollard[27] used such vortices as a model of coherent structures. In the present simulation a model of longitudinal viscous vortex is used, in which the tangential velocity is defined by $u_T^+ = (\Gamma^+/r^+)[1 - e^{-\alpha(r^+/a^+)^2}]$ where, in wall units, r^+ is the radial

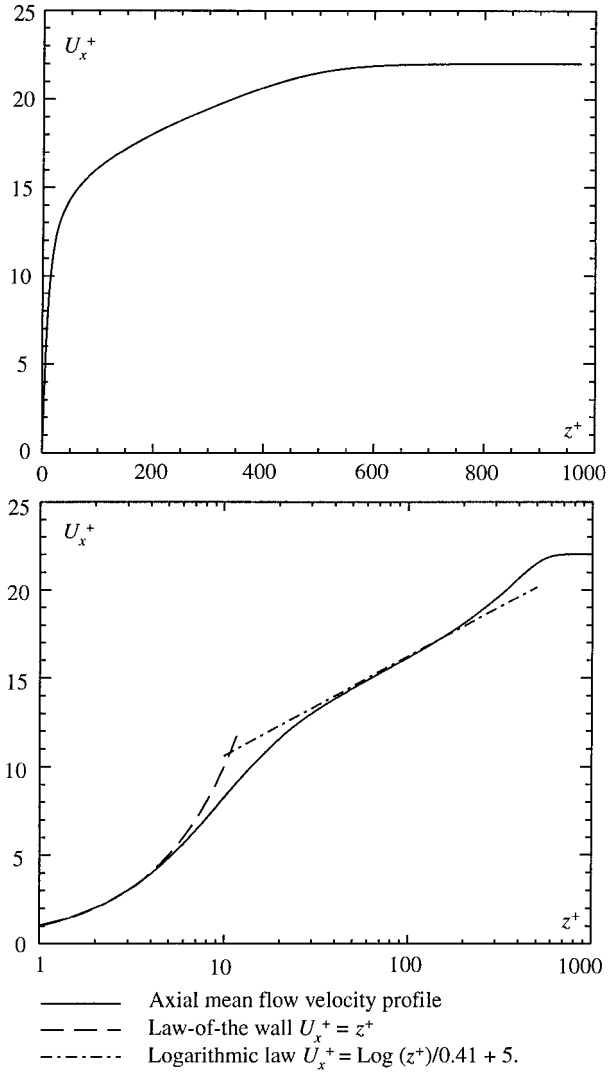

Fig. 2 Streamwise mean velocity profile injected at the inflow boundary ($x/H = -10$) (from Ref. 25).

distance in the yz plane from the vortex center, $\Gamma^+ = \Gamma/2\pi\nu$ is the vortex circulation with $|\Gamma^+| = 22$, $a^+ = 15$ is the vortex core radius, and $\alpha = 1.26$. One such vortex is centered at $z^+ = 30$ ($z/H = 0.66$) and $y^+ = 62.5$ ($y/H = 1.37$) with negative Γ^+. Three more vortices are constructed by a double symmetry through the vertical plane $y = 0$ and the horizontal plane $z = 0$.

A no-slip condition is applied on the solid wall surface. The flow is assumed to be periodic in the spanwise direction. On the other boundaries a zero-stress-like outflow condition is used, which was demonstrated to be efficient for separated flows.[28]

To ensure the time accuracy of the results, the normalized time step $\Delta t U_\infty / H$ is taken equal to 0.01, corresponding to 2000 time steps per vortex-sheddingcycle. During an initial phase of 4000 time steps, the computation corresponds to a DNS, the SGS model being disabled. At this time the flow is stationary and symmetrical through the plane $z = 0$. Then a perturbation of the velocity component u_z with an amplitude equal to U_∞ is imposed at one grid point during a single time step to onset the nonstationarity of the flow. An initial phase of 15,000 time steps was necessary before the flow was fully developed. The computation was then performed over 50,000 time steps, or a normalized time of 500, approximatively equal to 25 periods of trailing-edge vortex shedding. The total computation cost was 400 CPU h on a Cray YMP computer. The storage domains were selected with regard to the requirements of acoustic computations:

1) Wall-pressure fluctuations on the lower and upper plate sides near the trailing edge ($-3 \le x/H \le 0$) and on the blunt trailing edge.

2) Velocity component fluctuations in a cubic volume embedding the trailing edge ($-2.5 \le x/H,\ y/H,\ z/H \le +2.5$).

III. Analysis of Aerodynamic Data

A. Velocity Field

Figure 3 compares the initial mean velocity profile U_x/U_∞ at the inflow boundary ($x/H = -10$) to profiles (averaged in the spanwise direction) observed at four streamwise stations near the trailing edge ($x/H = -2.6, -1.8, -1.0, -0.2$). This plot indicates that the mean flow remains basically unaffected, except very close to the trailing edge, where the vortex shedding has strong effects. Figure 3 also plots turbulence intensity profiles $\sqrt{\langle u_x^2 \rangle}/U_\infty$, $\sqrt{\langle u_y^2 \rangle}/U_\infty$, and $\sqrt{\langle u_z^2 \rangle}/U_\infty$ at the same stations ($x/H = -2.6, -1.8, -1.0, -0.2$) and averaged in the spanwise direction. These turbulence intensity profiles are compared to those resulting from Spalart's computation of a fully developed TBL at $Re_\theta = 1410$. This comparison shows that, except very close to the plate's trailing edge ($x/H = -0.2$), the turbulence intensity of the computed flow remains much smaller than typical values encountered in TBLs: these results confirm that the computed flow remains laminar on the whole length of the flat plate. Very close to the trailing edge, the backward-facing step generates turbulence and vortex shedding, leading to a sudden growth

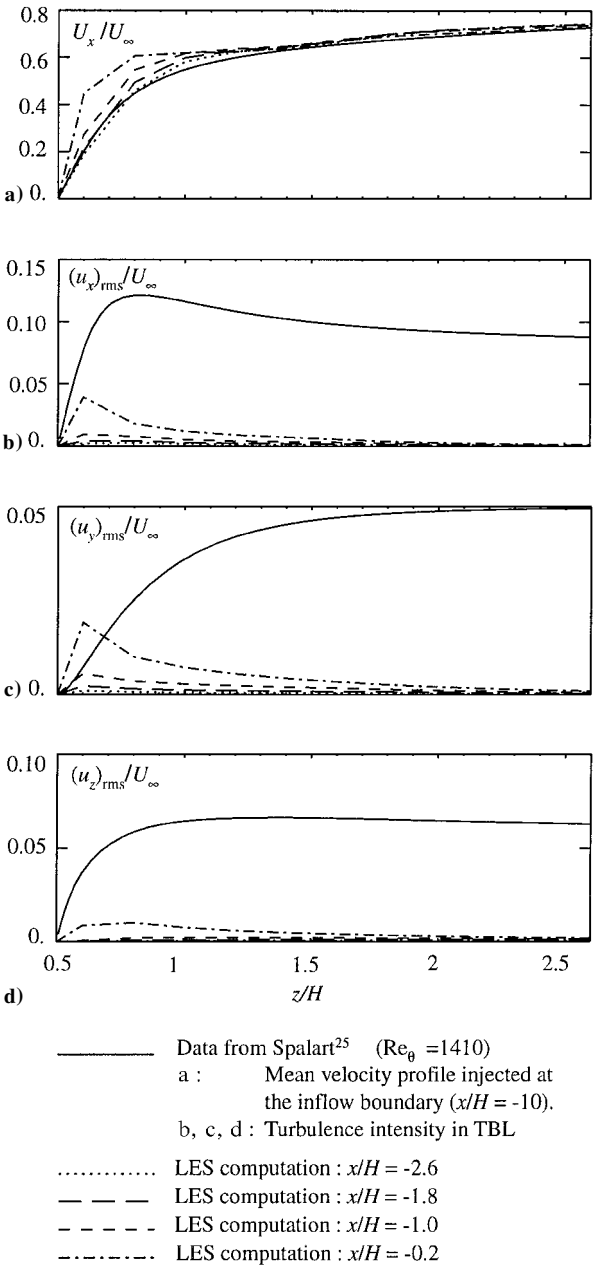

Fig. 3 Evolution of a) mean velocity profile and b) $\sqrt{\langle u_x^2 \rangle}/U_\infty$, c) $\sqrt{\langle u_y^2 \rangle}/U_\infty$, and d) $\sqrt{\langle u_z^2 \rangle}/U_\infty$ turbulence intensity profiles from the inflow boundary ($x/H = -10$) up to the trailing edge ($x/H = -0.2$): comparison of LES results to typical values in a fully developed TBL.[25]

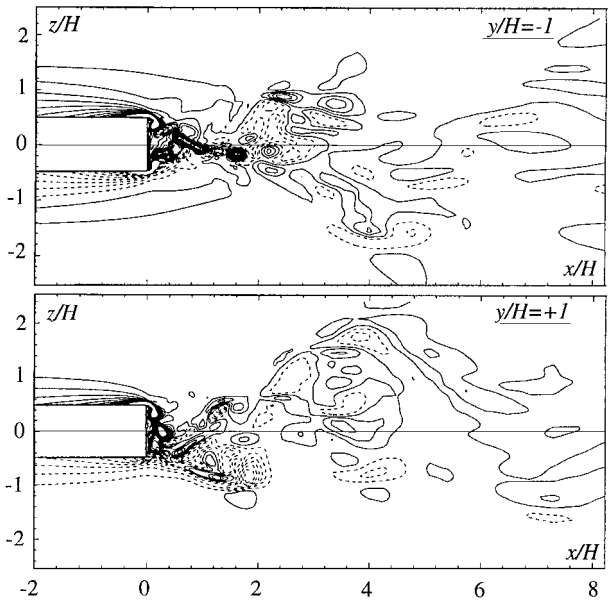

Fig. 4 Isocontours of the instantaneous spanwise vorticity ω_y (——, $\omega_y > 0$, and - - - -, $\omega_y < 0$): $t = 320\,H/U_\infty$.

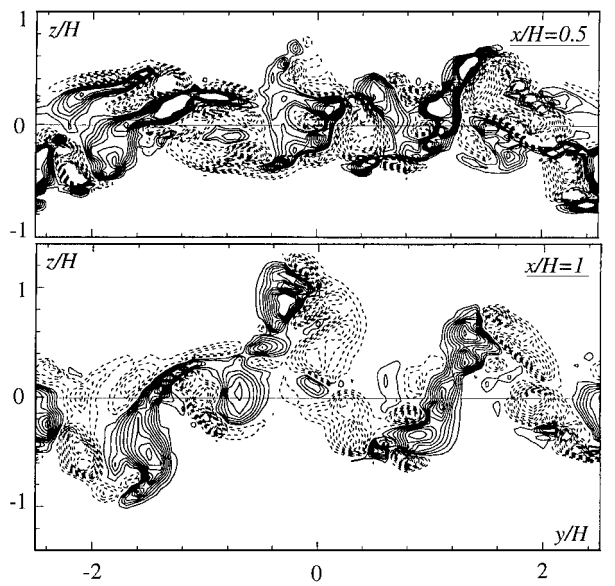

Fig. 5 Isocontours of the instantaneous vorticity ω_x (——, $\omega_x > 0$, and - - - -, $\omega_x < 0$): $t = 320\,H/U_\infty$.

of the turbulence intensities. A direct consequence of this feature is that the wall pressure and fluid velocity fluctuations around the trailing edge are entirely generated by the vortex-shedding mechanism, without any contribution from the laminar boundary layer.

Figure 4 shows isocontours of the instantaneous spanwise vorticity ω_y around the trailing edge at time $320H/U_\infty$ in the xz section located at $y/H = -1$ (top) and $y/H = +1$ (bottom). Small structures are exhibited near the plate's corners, because of the transition of the shear layers issuing from the corners, and just behind the trailing edge. Larger structures are shed from the trailing edge, as seen in the $y/H = +1$ section, which contribute to the vortex-shedding mechanism. In his unified theory of trailing-edge noise, Howe[1] emphasizes that this vorticity component ω_y (parallel to the edge of the plate) mainly contributes to the radiated noise, which is confirmed by the Ffowcs Williams–Hall theory recalled hereafter.

Figure 5 shows isocontours of the instantaneous streamwise vorticity ω_x in the trailing-edge wake at the same time as in the yz section located at $x/H = 0.5$ (top) and $x/H = 1$ (bottom). These plots show the strongly three-dimensional behavior of the flow in the wake, which consists of small structures (see the $x/H = 0.5$ view) stretched downstream (see the $x/H = 1$ view) with alternating vorticity sign.

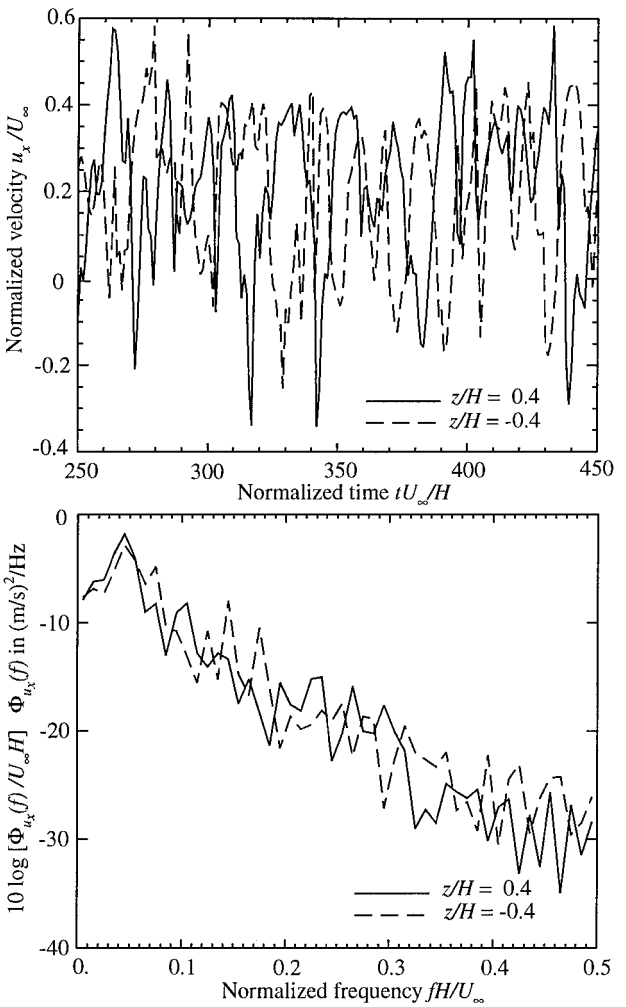

Fig. 6 Time history (top) and frequency spectra (bottom) of the streamwise velocity component in the wake at positions $x/H = 0.4$, $y/H = 0$, and $z/H = \pm 0.4$.

Figure 6 (top) shows the time history of the streamwise velocity component in the wake just behind the trailing edge ($x/H = 0.5$, $y/H = 0$, $z/H = \pm 0.4$), exhibiting a normalized periodicity $TU_\infty/H \approx 20$ or a normalized frequency $fH/U_\infty \approx 0.05$, as confirmed by the frequency spectra of these signals shown in the same figure (bottom). This frequency corresponds to a Strouhal number $ft_w/U_\infty \approx 0.25$ (based on the wake thickness $t_w = H + 2\delta^*$), in agreement with the experimental literature on trailing-edge vortex shedding.[2,3,29] The alternating vortex shedding is demonstrated by the phase opposition between the two signals ($z/H = \pm 0.4$) in Fig. 6 (top).

B. Wall-Pressure Field

Figure 7 (top) shows the time history of the wall pressure on the lower and upper sides of the plate at $x/H = -1$, i.e., at a distance H upstream of the trailing edge and at the spanwise location $y/H = +1$. As already mentioned for velocity fluctuations, this plot demonstrates a phase opposition between the opposite sides of the plate, resulting from alternating vortex shedding in the wake.

Figure 7 (bottom) shows single-point wall-pressure spectra at five streamwise locations ($x/H = -3, -2, -1, -0.5, 0$) along the axis ($y/H = 0$) of the upper side of the plate. These spectra clearly exhibit maxima around $fH/U_\infty = 0.05$, and their amplitudes rapidly decrease in the upstream direction.

Figure 8 shows the streamwise variation of the normalized rms wall pressure $\langle p^2 \rangle / (\rho U_\infty^2)^2$, averaged in the spanwise direction. This

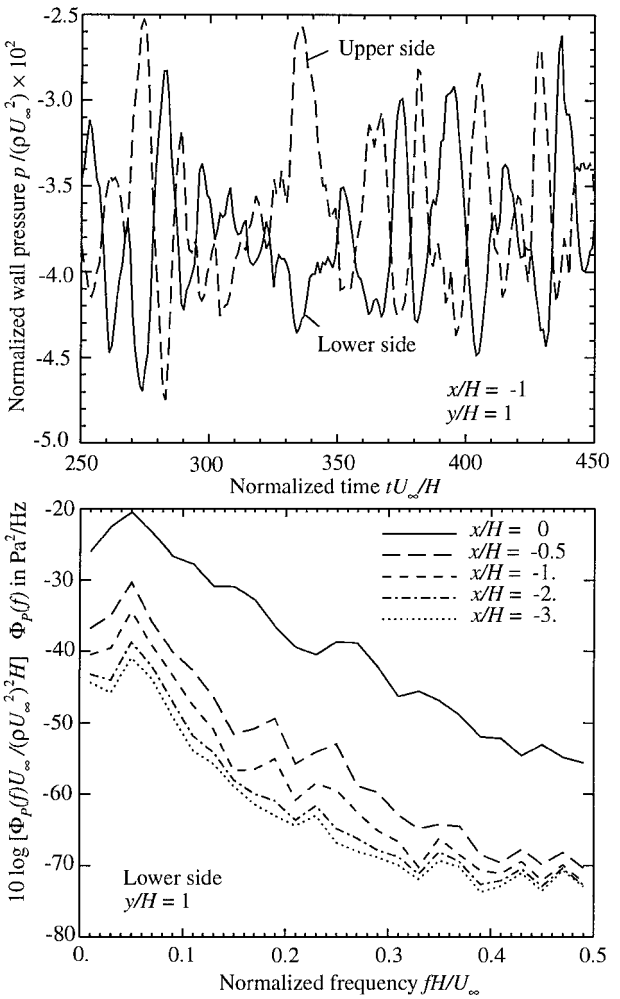

Fig. 7 Wall pressure fluctuations. Top: time history on both sides of the plate at $x/H = -1$ and $y/H = +1$. Bottom: spectra at five streamwise locations along the axis ($y/H = 0$) of the lower side of the plate.

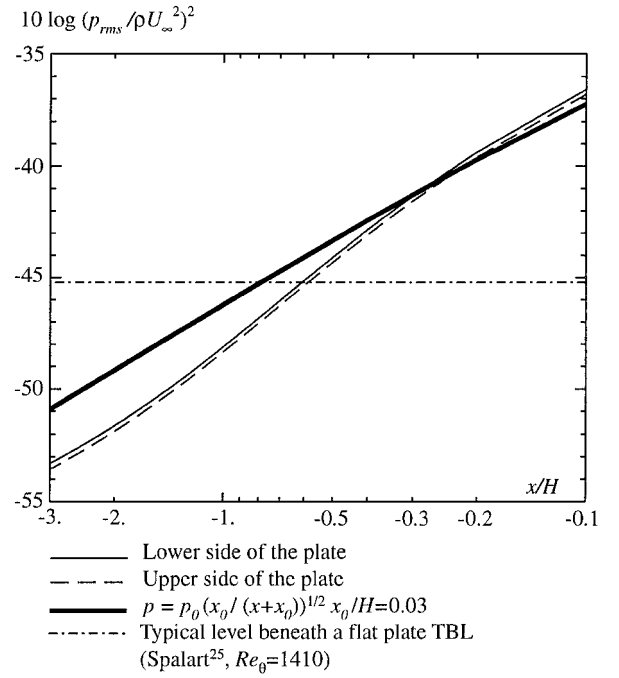

Fig. 8 Streamwise variation of the normalized rms wall-pressure fluctuations $\langle p^2\rangle/(\rho U_\infty^2)^2$, averaged in the spanwise direction, with respect to the distance x/H from trailing edge. Comparison to Blake's $x^{(-1/2)}$ law[29] and to a typical value ($\approx 3 \times 10^{-5}$) observed beneath a flat plate TBL of any thickness.

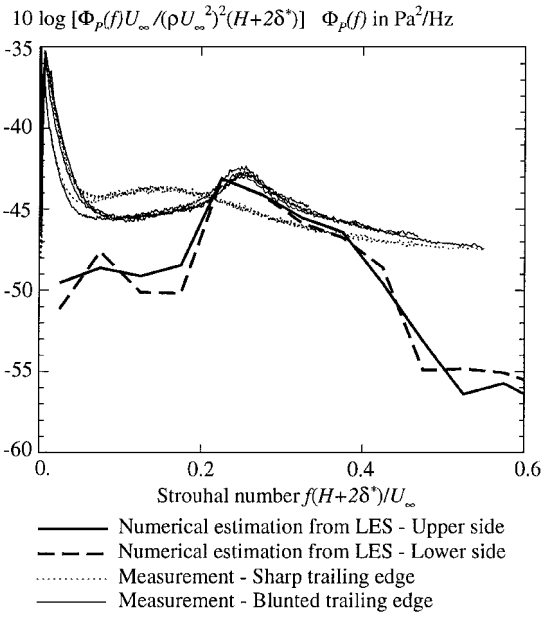

Fig. 9 Comparison of wall-pressure spectra near the trailing edge: 1) numerical estimation from LES on both sides of the flat plate, and 2) measurements on a NACA 12 airfoil with sharp and blunted trailing edges at various wind velocities (60–97 m/s) (from Ref. 3).

quantity is found to decrease as the inverse square root of the distance from the trailing edge, as was already observed experimentally,[3] and also predicted by a theoretical model developed by Blake[29] using conformal mapping of a simplified vortex street system behind a semi-infinite plane. If the upstream boundary layer were fully turbulent, $\langle p^2\rangle/(\rho U_\infty^2)^2$ would converge (in the upstream direction) to a typical value ($\approx 10^{-5}$) commonly observed beneath a flat-plate TBL of any thickness. For example, in his DNS of a fully developped TBL at $Re_\theta = 1410$, Spalart found $\langle p^2\rangle/(\rho U_\infty^2)^2 \approx 3 \times 10^{-5}$ (see Fig. 14 in Ref. 25). This level is schematically displayed on Fig. 8 as a dashed line, showing that the wall-pressure fluctuations induced by vortex shedding would exceed the fluctuations induced by the TBL only in a very narrow region ($0 < x/H < 1$) in the vicinity of the trailing edge.

Figure 9 presents wall-pressure spectra measured near the trailing edge of a NACA12 airfoil (chord: 0.5 m, span: 3 m) in the open jet (diameter: 2 m) of the ONERA's CEPRA 19 anechoic wind tunnel.[3] The airfoil trailing edge was equipped with a spanwise array of 9 pinhole transducers having a diameter of 1 mm, spaced 3 mm apart. The whole array was located 3 mm from the trailing edge. This instrumented area (covering a spanwise length of 0.1 m) was equipped with either a sharp or a blunted trailing edge ($H =$ 2.5 mm). The Reynolds number Re_H was around 10^4. The spectra shown in Fig. 9 were measured with both sharp and blunted trailing edges at wind velocities 60, 70, 80, and 97 m/s, by averaging the spectra of the nine transducers. The normalization involving the variables U_∞ and t_w provides a good collapse of the spectra measured at various wind velocities. These results clearly show the bluntness effect, with a bump rising at the normalized vortex shedding frequency $f t_w / U_\infty$.

The pressure fluctuations measured by the transducers were numerically simulated by averaging the wall pressure computed by LES in the area covered by the transducer. The corresponding spectra obtained on both sides of the plate are compared to measured spectra in Fig. 9. They are in good agreement with experimental spectra in the frequency region of the vortex shedding. Outside this frequency band the experimental spectra are dominated by the TBL pressure fluctuations, which are absent from the LES results, because of the steady inflow condition.

IV. Radiated Noise

A. Experimental Reference

Numerical simulations have limited intrinsic interest without qualitative and/or quantitative reference, and so it appeared essential

to confront the following numerical noise prediction with experimental data. Such a confrontation only aims at providing a rough qualitative and quantitative evaluation of the noise levels and frequency bands exhibited by the numerical approach.

The ONERA airfoil noise experiment just described was not suitable to this purpose because, in this experiment, the spanwise extent of the airfoil blunted trailing edge was only 0.1 m, or less than 5% of the entire airfoil span immersed in the flow, and, as a consequence, the noise radiated in the far field by the blunt trailing edge did not significantly differ from the broadband noise emitted by the sharp trailing edge.

Another airfoil noise experiment was conducted in 1980 at NASA in a quiet flow facility.[2] In this experiment a NACA 0012 airfoil with a 0.6-m chord and a 0.46-m span was successively equipped with full span sharp and blunted ($H = 2.5$ mm) trailing edges. Figure 10 (from Ref. 2) presents noise spectra measured with the airfoil equipped with either the sharp or the blunted trailing edge. The bluntness effect is clearly demonstrated, with a bump at the vortex-shedding frequency emerging up to 10 dB above the broadband spectrum. This result suggests that this experiment is particularly well suited to the validation of a vortex-shedding noise prediction.

B. Parameters of the Predictions

The following formulations are written with dimensional variables but were actually used in similar normalized forms obtained by scaling the space variables by H, the velocity by U_∞, the frequency by U_∞/H (or U_∞/t_w), and the pressure by the dynamic pressure ρU_∞^2. To compare the measured data with the numerical predictions, these are normalized in the same way using ρU_∞^2 and the Strouhal number $f t_w/U_\infty$. In the numerical prediction the location of the field point $\boldsymbol{x}$ with respect to the plate's trailing edge corresponds to the position of the microphone used to obtain the experimental spectra presented in Fig. 10 (distance $R = 1.2$ m or $R/H = 480$ from the trailing edge in a direction normal to the airfoil). Furthermore, because of the limited spanwise extent of the LES computation domain ($5H$), the flow around the whole span of the tested airfoil (0.46 m or $184H$) is artificially generated using the spanwise periodicity of the computed velocity field.

C. Lighthill Acoustic Analogy

Lighthill[13,14] rewrote the complete Navier–Stokes equations for a compressible viscous flow in a wave-equation form suitable for estimation of the noise radiated by any quadrupole distribution $\rho u_i u_j$. The Helmholtz (harmonic) form of this equation is

$$\Delta p^* + k^2 p^* = -\left(\frac{\partial^2(\rho u_i u_j)}{\partial y_i \partial y_j}\right)^* \tag{6}$$

where * denotes the generalized time Fourier transform:

$$f^*(\omega) = \frac{1}{2\pi}\int_{-\infty}^{+\infty} f(t) e^{-i\omega t}\,\mathrm{d}t$$

Without any reflecting surfaces, as in the case of an open jet, the general exact solution of this equation can be expressed as

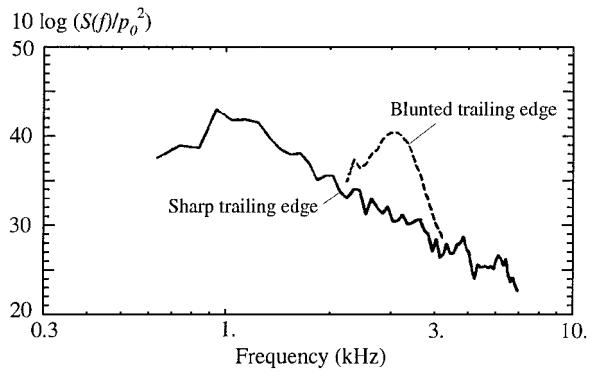

Fig. 10 NASA NACA12 airfoil trailing-edge noise measurements at wind velocity of 69.5 m/s for sharp and blunted ($H = 2.5$ mm) trailing edges (from Ref. 2).

$$p^*(\boldsymbol{x},\omega) = \frac{1}{4\pi}\frac{\partial^2}{\partial x_i \partial x_j}\iiint_{\vartheta}\frac{e^{-ikR}}{R}(\rho u_i u_j)^*\,\mathrm{d}V(\boldsymbol{y}) \tag{7}$$

where $R = |\boldsymbol{x} - \boldsymbol{y}|$. Integration must be performed on a volume ϑ containing all of the quadrupoles.

D. Curle's Solution

Curle[17] showed that a quadrupole volume integration over a given volume V is identical to a dipole integration over the surface S bounding volume V. With this assumption he developed an extension of the Lighthill solution (7) to flows including stationary bodies:

$$p^*(\boldsymbol{x},\omega) = \frac{1}{4\pi}\frac{\partial^2}{\partial x_i \partial x_j}\iiint_{\vartheta}\frac{e^{-ikR}}{R}(\rho u_i u_j)^*\,\mathrm{d}V(\boldsymbol{y}) - \frac{1}{4\pi}\frac{\partial}{\partial x_i}\iint_{\sigma}\frac{e^{-ikR}}{R} f_i^*\,\mathrm{d}S(\boldsymbol{y}) \tag{8}$$

where the volume integration is performed on a volume ϑ containing all of the quadrupoles and the surface integration is performed on any solid surface σ embedded in the volume ϑ, exerting forces per unit area f_i on the fluid.

By using the classical properties of functions of the retarded time $(t - R/c)$, the derivatives with respect to observation coordinates x_i are easily replaced by derivatives with respect to time. In the frequency domain Eq. (8) has the convenient form

$$p^*(\boldsymbol{x},\omega) = -\frac{1}{4\pi}\iiint_{\vartheta}\frac{R_i R_j}{R^2}\frac{e^{-ikR}}{R}k^2\left(1 + 0\left(\frac{1}{kR}\right)\right)(\rho u_i u_j)^*\,\mathrm{d}V(\boldsymbol{y}) + \frac{i}{4\pi}\iint_{\sigma}\frac{R_i}{R}\frac{e^{-ikR}}{R}k\left(1 + 0\left(\frac{1}{kR}\right)\right)f_i^*\,\mathrm{d}S(\boldsymbol{y}) \tag{9}$$

where $R_i = x_i - y_i$. In the far-field configuration corresponding to the spectra on Fig. 10 ($M = 0.2$, $R/H = 480$), the terms between brackets are close to unity ($kR \approx 30$ at the vortex shedding frequency $f = 0.05$).

Figure 11 presents the noise spectrum computed from LES data using Curle's formulation (9). In this presentation the quadrupolar and dipolar contributions to the total radiated noise are compared. The noise is mostly generated by pressure fluctuations, confirming that quadrupoles in free field are inefficient noise radiators. The same plot displays the normalized spectrum of Fig. 10 corresponding to the blunt trailing edge. This comparison suggests that, in the frequency domain of the vortex-shedding mechanism, predicted levels are consistent. This experimental spectrum is plotted only in the frequency domain in which the noise is generated by the vortex-shedding mechanism. Outside this frequency domain, the noise is caused by the acoustic diffraction of the TBL on the trailing edge, without regard to the trailing-edge bluntness.

E. Ffowcs Williams and Hall's Theory

The preceding result using Curle's formulation is mostly governed by the flow-induced or hydrodynamic wall-pressure fluctuations localized on a very narrow strip along the trailing edge. In that context the upstream geometry of a (virtual) airfoil is absent, and the possible acoustic reflections on the airfoil walls are not taken into account. The theory developed by Ffowcs Williams and Hall[18] offers an interesting alternative to this. These authors developed a formulation of the noise generated by the acoustic scattering of turbulence passing over the edge of an infinite half-plane. Basically, this formulation is a solution of Lighthill's equation (6) involving the acoustic Green's function $G(\boldsymbol{x} \mid \boldsymbol{y}, \omega)$ of the specific geometry under consideration. This function is the solution of $(\Delta + k^2)G = -4\pi\,\delta(\boldsymbol{x} - \boldsymbol{y})$ whose normal derivative vanishes on the solid walls. By using such a Green's function, the radiated sound becomes

$$p^*(\boldsymbol{x},\omega) = \frac{1}{4\pi}\iiint_{\vartheta}(\rho u_i u_j)^*\frac{\partial^2 G}{\partial y_i \partial y_j}\,\mathrm{d}V(\boldsymbol{y}) \tag{10}$$

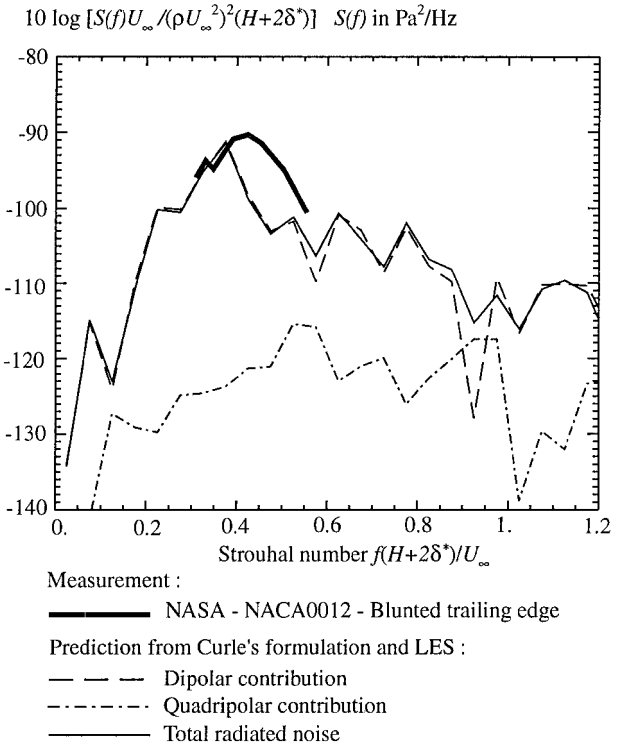

Fig. 11 Noise spectra computed from LES data using Curle's computation (comparison of quadrupolar and dipolar terms). Comparison with measured spectra (from Ref. 2).

The observation point $\boldsymbol{x}(r, \theta, z)$ and the source point $\boldsymbol{y}(r_0, \theta_0, z_0)$ are now defined in cylindrical coordinates, with the cylindrical axis parallel to the plane edge. A far-field ($r \gg r_0$) approximation of $G(\boldsymbol{x} \mid \boldsymbol{y}, \omega)$ for an infinite half-plane was given by Macdonald,[30] using Fresnel's function

$$F(x) = \frac{e^{-i\pi/4}}{\sqrt{\pi}} \int_{-\infty}^{x} e^{iu^2}\, \mathrm{d}u$$

$$G(\boldsymbol{x} \mid \boldsymbol{y}, \omega) = \frac{e^{-ikR}}{R} F(a) + \frac{e^{-ikR'}}{R'} F(a') \tag{11}$$

where $R = |\boldsymbol{x} - \boldsymbol{y}|$ and $R' = |\boldsymbol{x} - \boldsymbol{y}'|$. $\boldsymbol{y}'(r_0, -\theta_0, z_0)$ is the mirror point of $\boldsymbol{y}$ through the extended half-plane and $a, a' = \sqrt{(2kr_0 \sin\phi)} \cos[(\theta \pm \theta_0)/2]$. For quadrupoles that are well within a wavelength of the edge or that satisfy the condition $2kr_0 \ll 1$, Fresnel's function simplifies into

$$F(x) = \tfrac{1}{2} + (e^{-i\pi/4}/\sqrt{\pi})[x + O(x^3)]$$

The resulting simplified expression for $G(\boldsymbol{x} \mid \boldsymbol{y}, \omega)$ is introduced in an expansion of $(\rho u_i u_j)^* (\partial^2 G / \partial y_i \partial y_j)$ in cylindrical coordinates to provide the following expression of the radiated noise:

$$p^*(\boldsymbol{x}, \omega) = \frac{\rho k^2 e^{-i\pi/4}}{2\pi^{\frac{3}{2}}} \cos\left(\frac{\theta}{2}\right) \int \sqrt{\sin\phi}\, \frac{e^{-ikR}}{R} (2kr_0)^{-\frac{3}{2}}$$

$$\times \left\{ \left[(u_\theta^2)^* - (u_r^2)^* \right] \cos\left(\frac{\theta_0}{2}\right) + 2(u_r u_\theta)^* \sin\left(\frac{\theta_0}{2}\right) \right\} \mathrm{d}V(\boldsymbol{y}) \tag{12}$$

In this volume calculation the contribution of each quadrupole is affected by the $(2kr_0)^{-3/2}$ term, where r_0 is the distance of the quadrupole from the trailing edge. Consequently, the most important contribution to the radiated noise comes from the quadrupoles closest to the trailing edge. Quadrupoles involving the spanwise velocity component u_z do not appear in Eq. (12) because their contribution to the radiated noise is of a smaller order of magnitude.

The application of this theory to the case of a thick plate is not straightforward, as modeling of the plate by a zero-thickness half-plane raises several questions. Acoustically speaking, the question of the plate thickness assumes rather different aspects, depending on whether wave scattering or wave generation is concerned. In the first case the scattering of incoming acoustic waves is obviously not affected by the edge geometry insofar as its thickness is negligible compared to the acoustic wavelength. Noise generation caused by turbulence interacting with geometrical singularities is a different problem. It is known (see, for example, Crighton's review[31]) that for an airfoil with a given chord (much larger than the wavelength) and wedge angle the radiated noise does not depend on the geometric details (much smaller than the wavelength) of the trailing edge. A dimensional analysis shows that turbulence passing at a distance r_0 from the edge of a wedge with an angle π/n generates sound proportional to $(kr_0)^{n-2}$ (with the half-plane case corresponding to $n = \frac{1}{2}$), the main governing parameter being the wedge angle without regard to the small details of the trailing-edge geometry. However, this is certainly not the case if the aerodynamic unsteady near field is governed by the small-scale geometry of the trailing edge. To illustrate this, Fig. 12 provides a localization of the main quadrupole sources $(u_x^2)^*$ obtained by LES in an xz plane at the vortex-shedding frequency, revealing that the strongest quadrupoles are located just downstream of the two corners of the thick plate. This shows that the near-field source distribution is strongly related to the local geometry of the trailing edge and suggests that, conversely, the location of wall singularities can affect the acoustic diffraction of local quadrupoles.

This was numerically checked by modeling the thick plate by a horizontal zero-thickness infinite half-plane with the edge located at $x/H = 0$ and $z/H = 0$ and applying formulation (12) to the LES data. As expected, the resulting noise spectrum is in poor agreement with measurements (see Fig. 13), with low power in the vortex-shedding frequency band. In addition, the particular source distribution presented in Fig. 12 gave the idea of separately simulating the quadrupolar acoustic diffraction occurring on each corner of the plate. This was achieved by modeling the thick plate by a single horizontal zero-thickness half-plane with its edge located either at the upper corner of the plate ($x/H = 0$ and $z/H = 0.5$) or the lower corner of the plate ($x/H = 0$ and $z/H = -0.5$). As can be seen in Fig. 13, this method produces better qualitative and quantitative results, with noise spectra relatively close to the results obtained from Curle's formulation. This fairly good agreement with measurements and with Curle's theory may strengthen the hypothesis that the trailing edge of a thick plate acts as a double-singularity

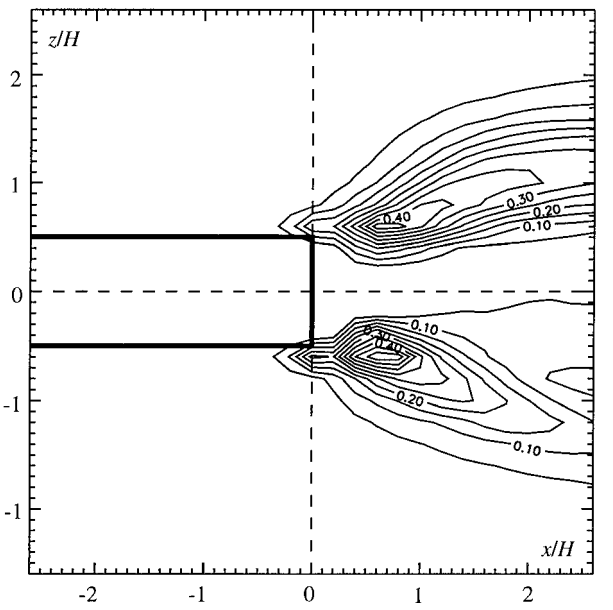

Fig. 12 Isocontours in the xz plane of $(u_x^2)^*$ taken at the vortex-shedding frequency (averaged in the y spanwise direction).

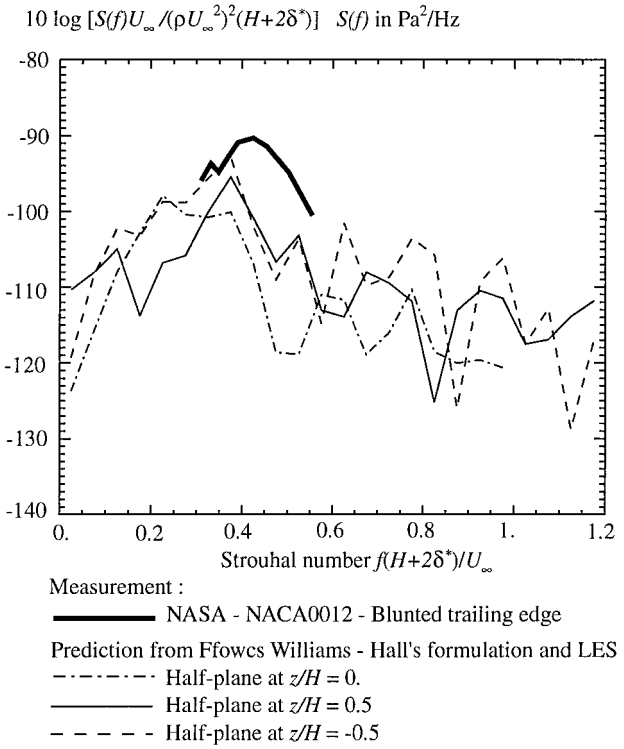

Fig. 13 Noise spectra computed from LES data using Ffowcs Williams–Hall's formulation and simulating the thick plate by a single half-plane located at $z/H = 0$, $+0.5$, and -0.5. Comparison with measured spectrum (from Ref. 2).

system involving two separate turbulence scattering mechanisms occurring on each corner of the plate.

This result obviously relies on the strong assumptions underlying the model of a thick plate by a zero-thickness surface. However, this approach is interesting because it provides an estimate of the radiated noise, which takes into account the acoustic diffraction by a (simplified) airfoil. This approach also offers the opportunity to compare two different formulations deriving from Lighthill's analogy.

V. Conclusions

In this work the LES of trailing-edge flow is performed with the specific purpose of an application to the computation of radiated noise using Lighthill's acoustic analogy. The aerodynamic results clearly demonstrate the strongly three-dimensional character of the flow, with the onset of a vortex-shedding mechanism occurring at a frequency in agreement with theoretical and experimental data. The pressure field generated on the trailing-edge walls is analyzed in detail. Its amplitude, frequency, and streamwise evolution compare favorably with data measured near the trailing edge of an airfoil. LES data are used to compute the radiated acoustic field using Curle's solution of Lighthill's equation. Despite the significant difference between the experimental and numerical Reynolds numbers, this noise prediction compares favorably with measurements of the noise radiated by an airfoil with a blunt trailing edge in a quiet flow facility. Finally, the theory developed by Ffowcs Williams and Hall is considered. This formulation expresses the noise generated by turbulence passing over the edge of an infinite half-plane. The application of this theory to a thick trailing edge is admittedly controversial, but following a close examination of the quadrupole source distribution around the trailing edge, interesting results were obtained by separately simulating the quadrupolar acoustic diffraction occurring on each corner of the plate.

Several aspects of this study suggest further work.

As far as LES is concerned, there is already a demand for computing unsteady flows around more complex geometries. In the context of acoustic applications, this will probably be made possible only with the development of new techniques that integrate time filtering such as the very large eddy simulation. Even with less complicated flows like the present one, the need for better insight into the three-dimensional effects and more realistic comparisons with experiments will justify the spanwise extension of the computation domain and computations at higher Reynolds numbers. This supposes an increase in the number of mesh points, with the ensuing hardware and algorithm difficulties. Another topic of research addresses the generation of realistic LES inflow conditions, which were steady in the present work, making the broadband noise resulting from TBL acoustic diffraction impossible to predict. Promising techniques include previous LES or unsteady RANS computations or new approaches consisting of simulating the velocity fluctuations by a linear stochastic estimation procedure.

Concerning the acoustic prediction methods used or discussed in this paper, it is still uncertain whether they are able to integrate correctly the effects of acoustic reflections on the solid surface of an actual airfoil or wing. Curle's formulation involves only the solid surfaces where hydrodynamic pressure fluctuations are known, and Ffowcs Williams–Hall's formulation simulates it by an infinite half-plane. This difficulty could be resolved in the near future by coupling Lighthill's classical formulation with a numerical acoustic Green's function computed using the boundary element method to discretize the exact geometries. Feasability studies are already being undertaken in this direction. Moreover, the noise predictions used herein do not take into account the convection effect that affects experimental data. Finally, another field of promising methods in CAA is based on the coupling of a compressible Navier–Stokes solver and Kirchhoff surface techniques or an Euler's linearized equations solver.

Acknowledgments

This work was supported by Direction Générale pour l'Armement/Direction des Recherches et Études Techniques, French Ministry of Defense. Part of this work was presented at the First Air Force Office of Scientific Research International Conference on DNS and LES at Ruston, Louisiana, in August 1997 (Ref. 16).

References

[1]Howe, M. S., "A Review of the Theory of Trailing Edge Noise," *Journal of Sound and Vibration*, Vol. 61, No. 3, 1978, pp. 437–465.

[2]Brooks, T. F., and Hodgson, T. H., "Prediction and Comparison of Trailing Edge Noise Using Measured Surface Pressures," *Journal of Sound and Vibration*, Vol. 78, No. 1, 1981, pp. 69–117.

[3]Garcia, P., "Airfoil Noise in a Uniform Flow," *La Recherche Aérospatiale* (English version), Vol. 3, 1989, pp. 1–7.

[4]Mitchell, B. E., Lele, S. K., and Moin, P., "Direct Computation of the Sound from a Compressible Co-Rotating Vortex Pair," *Journal of Fluid Mechanics*, Vol. 285, 1995, pp. 181–202.

[5]Colonius, T., Lele, S. K., and Moin, P., "Sound Generation in a Mixing Layer," *Journal of Fluid Mechanics*, Vol. 330, 1997, pp. 375–409.

[6]Tam, C. K. W., "Computational Aeroacoustics: Issues and Methods," *AIAA Journal*, Vol. 33, No. 10, 1995, pp. 1788–1796.

[7]Lele, S. K., "Computational Aeroacoustics: A Review," AIAA Paper 97-0018, Jan. 1997.

[8]Lyrintzis, A. S., and Mankbadi, R. R., "On the Prediction of the Far-Field Jet Noise Using Kirchhoff's Formulation," AIAA Paper 95-0508, June 1995.

[9]Mankbadi, R. R., Hayer, M. E., and Povinelli, L. A., "Structure of Supersonic Jet Flow and Its Radiated Sound," *AIAA Journal*, Vol. 32, No. 5, 1994, pp. 897–906.

[10]Wang, M., Lele, S. K., and Moin, P., "Computation of Quadrupole Noise Using Acoustic Analogy," *AIAA Journal*, Vol. 34, No. 11, 1996, pp. 2247–2254.

[11]Wang, M., Lele, S. K., and Moin, P., "Sound Radiation During Local Laminar Breakdown in a Low-Mach-Number Boundary Layer," *Journal of Fluid Mechanics*, Vol. 319, 1996, pp. 197–218.

[12]Bastin, F., Lafon, P., and Candel, S., "Computation of Jet Mixing Noise due to Coherent Structures: The Plane Jet Case," *Journal of Fluid Mechanics*, Vol. 335, 1997, pp. 261–304.

[13]Lighthill, M. J., "On Sound Generated Aerodynamically. I. General Theory," *Proceedings of the Royal Society of London, Series A*, Vol. 211, 1952, pp. 564–587.

[14]Lighthill, M. J., "On Sound Generated Aerodynamically. II. Turbulence as a Source of Sound," *Proceedings of the Royal Society of London, Series A*, Vol. 222, 1954, pp. 1–32.

[15]Manoha, E., Troff, B., and Sagaut, P., "Trailing Edge Noise Prediction Using Large Eddy Simulation and Acoustic Analogy," AIAA Paper 98-1066, Jan. 1998.

[16]Troff, B., Manoha, E., and Sagaut, P., "LES of Trailing-Edge Flow with Application to Radiated Noise," *Advances in DNS/LES*, edited by C. Liu and Z. Liu, Greyden, Columbus, OH, 1997, pp. 589–596.

[17]Curle, N., "The Influence of Solid Boundaries upon Aerodynamic Sound," *Proceedings of the Royal Society of London, Series A*, Vol. 231, 1952, pp. 505–514.

[18]Ffowcs Williams, J. E., and Hall, L. H., "Aerodynamic Sound Generation by Turbulent Flow in the Vicinity of a Scattering Half Plane," *Journal of Fluid Mechanics*, Vol. 40, 1970, pp. 657–670.

[19]Sagaut, P., Troff, B., Lê, T. H., and Ta, P. L., "Large Eddy Simulation of Turbulent Flow Past a Backward Facing Step with a New Mixed Scale SGS Model," *Computation of Three-Dimensional Complex Flows*, Vol. 53, Notes on Numerical Fluid Mechanics, edited by M. Deville, S. Gavrilakis, and I. Rhyming, Vieweg, Brunswick, Germany, 1996, pp. 271–278.

[20]Sagaut, P., Lê, T. H., and Loc, T. P., "Numerical Investigations of the Flow Around a Square Cylinder via Large Eddy Simulation," *Computational Fluid Dynamics '96*, edited by J. Désidéri, C. Hirsch, P. Le Tallec, M. Pandolfi, and J. Périaux, Wiley, New York, 1996, pp. 897–903.

[21]Sagaut, P., "Simulations of Separated Flows with Subgrid Models," *La Recherche Aerospatiale* (English version), Vol. 1, 1996, pp. 51–63.

[22]Lê, T. H., Troff, B., Sagaut, P., Dang-Tran, K., and Ta, P. L., "PEGASE: A Navier–Stokes Solver for Direct Numerical Simulation of Incompressible Flows," *International Journal for Numerical Methods in Fluids*, Vol. 24, No. 9, 1997, pp. 833–861.

[23]Van der Vorst, H., "Bi-CGSTAB: A Fast and Smoothly Converging Variant of Bi-CG for the Solution of Nonsymmetric Linear Systems," *SIAM Journal on Scientific Statistical Computing*, Vol. 13, No. 2, 1992, pp. 631–644.

[24]Rodi, W., Ferziger, J. H., Breuer, M., and Pourquié, M., "Status of Large Eddy Simulation: Results of a Workshop," *Journal of Fluids Engineering*, Vol. 119, No. 2, 1997, pp. 248–262.

[25]Spalart, P. R., "Direct Simulation of a Turbulent Boundary Layer up to r_θ = 1410," *Journal of Fluid Mechanics*, Vol. 187, 1998, pp. 61–98.

[26]Smith, C. R., and Schwartz, S. P., "Observation of Streamwise Rotation in the Near-Wall Region of a Turbulent Boundary Layer," *Physics of Fluids*, Vol. 26, No. 3, 1983, pp. 641–652.

[27]Wakarami, N., and Pollard, A., "Three-Dimensional, Time Dependent, Transitional Flow over a Forward-Facing Step Including Near-Wall Structure," *Proceedings of the Ninth Symposium on Turbulent Shear Flows*, Vol. 2, 1993 (Paper 13-3).

[28]Sani, R. L., and Gresho, P. M., "Resume and Remarks on the Open Boundary Condition Minisymposium, 1994," *International Journal for Numerical Methods in Fluids*, Vol. 18, No. 10, 1994, pp. 983–1008.

[29]Blake, W. K., "A Near-Wake Model for the Aerodynamic Pressures Exerted on Singing Trailing Edges," *Journal of the Acoustical Society of America*, Vol. 60, No. 3, 1976, pp. 594–598.

[30]Macdonald, H. M., "A Class of Diffraction Problems," *Proceedings of the London Mathematical Society*, Vol. 2, No. 14, 1915, pp. 410–427.

[31]Crighton, D. G., "Basic Principles of Aerodynamic Noise Generation," *Progress in Aerospace Science*, Vol. 16, No. 1, 1975, pp. 31–96.

P. Givi
Associate Editor